AGU PUBLICATIONS

JGR

Journal of Geophysical Research: Solid Earth

RESEARCH ARTICLE
10.1002/2014JB011001

**Key Points:**
- Augment STZ theory with temperature depedent viscoplastic contact strength
- Investigate steady state and transient friction response of gouge
- Fit Sone and Shimamoto (2009) high-speed friction data

**Correspondence to:**
A. E. Elbanna,
elbanna2@illinois.edu

**Citation:**
Elbanna, A. E., and J. M. Carlson (2014), A two-scale model for sheared fault gouge: Competition between macroscopic disorder and local viscoplasticity, *J. Geophys. Res. Solid Earth*, *119*, 4841–4859, doi:10.1002/2014JB011001.

Received 29 JAN 2014
Accepted 3 MAY 2014
Accepted article online 9 MAY 2014
Published online 3 JUN 2014

# A two-scale model for sheared fault gouge: Competition between macroscopic disorder and local viscoplasticity

**A. E. Elbanna[1] and J. M. Carlson[2]**

[1]Department of Civil and Environmental Engineering, University of Illinois at Urbana-Champaign, Urbana, Illinois, USA, [2]Department of Physics, University of California, Santa Barbara, California, USA

**Abstract** We develop a model for sheared gouge layers that accounts for the local increase in temperature at the grain contacts during sliding. We use the shear transformation zone theory, a statistical thermodynamic theory, to describe irreversible macroscopic plastic deformations due to local rearrangements of the gouge particles. We track the temperature evolution at the grain contacts using a one-dimensional heat diffusion equation. At low temperatures, the strength of the asperities is limited by the flow strength, as predicted by dislocation creep models. At high temperatures, some of the constituents of the grains may melt leading to the degradation of the asperity strength. Our model predicts a logarithmic rate dependence of the steady state shear stress in the quasistatic regime. In the dense flow regime the frictional strength decreases rapidly with increasing slip rate due to thermal softening at the granular interfaces. The transient response following a step in strain rate includes a direct effect and a following evolution effect, both of which depend on the magnitude and direction of the velocity step. In addition to frictional heat, the energy budget includes an additional energy sink representing the fraction of external work consumed in increasing local disorder. The model links low-speed and high-speed frictional response of gouge layers and provides an essential ingredient for multiscale modeling of earthquake ruptures with enhanced coseismic weakening.

## 1. Introduction

Understanding the dynamics of shear weakening in gouge layers, under a wide range of slip rates and confining normal stresses, is a fundamental and long-standing challenge in earthquake source physics. In the case of mature faults that have accumulated hundreds of meters of slip throughout their active history, there is little doubt that shear deformation localizes to very thin zones typically less than 1 mm wide [*Chester et al.*, 1993; *Chester and Chester*, 1998; *Scholz*, 2002; *Chester et al.*, 2004; *Noda and Shimamoto*, 2005; *Lockner et al.*, 2000; *Ben-Zion and Sammis*, 2003]. The zone which accommodates most of the slip within this layer can be even smaller. The absence of significant evidence of melting [*Sibson*, 1973; *Lachenbruch*, 1980], despite the extreme localization of strain, suggests that fault friction must be low during dynamic sliding [*Kanamori and Heaton*, 2000]. The fact that the static strength of fault gouge satisfies Byerlee's law (static friction coefficient 0.6–0.9), however, indicates that faults are statically strong. Understanding the mechanisms of dynamic weakening, from high static friction to low sliding friction, is essential for developing more accurate models of earthquake ruptures and scenarios for ground motion prediction [*Rice*, 1980, 2006; *Heaton*, 1990; *Lapusta*, 2000; *Lapusta and Rice*, 2003; *Aagaard and Heaton*, 2008; *Ampuero and Ben-Zion*, 2008; *Noda et al.*, 2009, 2010].

In this paper, we present a two-scale model for dynamic weakening in gouge layers. Macroscopically, plastic strain results from the accumulation of local granular rearrangements. Microscopically, thermally activated viscoplastic processes at the grain contacts control sliding and force chain instabilities. The interplay between the two processes leads to nonmonotonic strain rate dependence for the shear strength.

Irreversible local rearrangements of gouge particles is modeled using the shear transformation zone (STZ) theory, a continuum model of plastic deformation in amorphous solids that quantifies local configurational disorder [*Falk and Langer*, 1998]. The basic assumption in the theory is that plastic deformation occurs at rare noninteracting localized spots known as shear transformation zones (STZs). An internal state variable, the effective temperature, describes fluctuations in the configurational states of the granular material (i.e., a measure of local entropy) and controls the density of STZs [*Langer*, 2004; *Haxton and Liu*, 2007; *Langer*

*and Manning*, 2008; *Bouchbinder and Langer*, 2009]. Effective temperature can be related to the system porosity [*Lieou and Langer*, 2012]. This approach coarse-grains granular simulations while retaining important physical concepts.

Gouge particles with dimensions of a micrometer and above are too big for thermal fluctuations to initiate transitions. Nonetheless, slip processes at the grain interfaces, such as dislocation glide and stable crack growth, are thermally activated [*Chester*, 1994, *Rice et al*., 2001; *Noda*, 2008]. In particular, the high confining pressure at depths relevant to earthquake nucleation and propagation lead to the prevalence of plastic conditions in the contact region. The local plastic rheology depends strongly on the local temperature. Moreover, at high slip rates, flash heating may occur leading to a significant degradation in the contact strength. Flash heating is the rapid increase in local temperature at the contact asperity due to heat generation arising from frictional sliding at a rate higher than the heat diffusion rate [*Rice*, 2006]. By including the effect of local temperature changes on the evolution of the flow strength at the particle interfaces, it is possible to interpret the nonmonotonic rate-dependent response of gouge layers observed experimentally at different slip rates and normal stresses [*Chester*, 1994; *Blanpied et al*., 1995; *Sone and Shimamoto*, 2009].

The important new contribution in this paper is the inclusion of a modified theory of flash heating within the framework of the STZ theory, and exploration of the consequences for laboratory friction measurements and earthquakes. Frictional weakening in sliding rock surfaces by flash heating was formulated by *Rice* [2006] and *Noda* [2008]. The latter proposed that the average contact temperature of the sliding surface acts as a state variable. The formulation proposed in this paper is more appropriate for gouge layers as the STZ theory enables us to capture some complexity associated with force chain dynamics that was not taken into account in previous models. In particular, the classical assumption that the sliding velocity at the contact asperities is equal to the imposed velocity is not generally true for gouge. The current theory provides a way to compute this velocity as a function of grain size and gouge compactivity. Moreover, our theory correctly takes into account the differences in stress states between a gouge layer of finite thickness and rock masses sliding on a mathematical plane. This is further discussed in section 8.

Modeling flash heating in sheared gouge layers through the inclusion of an accurate description of the microscopic contact temperature evolution provides a mechanism for (i) rate strengthening in the quasistatic regime of granular flow and (ii) rate weakening in the dense regime of granular flow. This has important geophysical implications for nucleation, dynamic rupture, and energy partitioning in earthquakes, as well as landslides, where flash heating has been proposed as an important weakening mechanism [*Lucas et al*., 2014]. The proposed theory is primarily relevant for small and moderate slips. For larger slips the rise in macroscopic temperature, under seismological conditions, will be large enough to cause macroscopic melting unless other weakening mechanisms such as pore fluid pressurization operate.

The remainder of the paper is organized as follows. In section 2 we review the basic elements of the STZ theory. In section 3 we discuss the model for local viscoplasticity at the grain contacts. In sections 4 and 5 we describe the procedure for calculating the contact temperature for both single and multiple contacts cases. In section 6 we discuss the parameter selection. In section 7 we investigate the predictions of the STZ theory for the steady state sliding shear stress as well as the transient behavior. We consider a wide range of strain rates. We also quantify the partition of dissipated energy between configurational and thermal components. In section 8 we discuss the implications of this model for dynamic rupture and gouge friction modeling. We summarize our conclusions in section 9.

## 2. A Review of the STZ Theory

STZ theory is a nonequilibrium statistical thermodynamic framework for describing plastic deformations in amorphous materials by quantifying local disorder. It has been applied to a variety of systems including granular fault gouge [*Daub and Carlson*, 2008; *Daub et al*., 2008; *Daub and Carlson*, 2010; *Hermundstad et al*., 2010], glassy materials [*Falk and Langer*, 1998, 2000; *Manning et al*., 2007, 2009], thin film lubricants [*Lemaitre and Carlson*, 2004], and hard spheres [*Lieou and Langer*, 2012]. The theory, with just a few parameters, has successfully reproduced a large number of experiments and molecular dynamics simulations for glassy materials, including strain localization patterns [e.g., *Langer and Manning*, 2007; *Manning et al*., 2007; *Lieou and Langer*, 2012; and the review papers by *Daub and Carlson*, 2010; *Falk and Langer*, 2010]. Recently, the theory was extended to model shear flows of granular materials with breakable particles [*Lieou et al*., 2014], as

well as acoustic fluidization under low normal stresses (C. K. C. Lieou et al., Shear flow of angular grains: Acoustic effects and nonmonotonic rate dependence of volume, submitted to *Physical Review E*, 2014). While the classical rate and state friction formulation has been successful in modeling the transient and steady state shear response under a variety of conditions [*Marone*, 1998], it is incapable of modeling these additional phenomena (such as grain breakage) which are known to have important implications on gouge response [e.g., *Mair and Abe*, 2011, and references therein; *Elst et al.*, 2012]. In that respect, the STZ theory possesses an advantage over the phenomenological approaches. On one hand, it is flexible enough to include the additional state variables required to model these phenomena; and on the other hand, it constrains the evolution of these state variables by the physics-based laws of statistical thermodynamics. In this section we review the basic assumptions and equations of this theory.

Granular particles can move and rearrange in response to applied stress. Molecular dynamics simulations of glassy materials reveal that plastic irreversible deformation is concentrated in localized regions called shear transformation zones (STZs). These regions undergo configurational rearrangement by flipping between two orientations, antialigned and aligned with the direction of principal shear stresses [*Falk and Langer*, 1998].

A single STZ transition is represented by an irreversible rearrangement that occurs within the STZ, whereby the particles locally exchange nearest neighbor relationships. This event generates a quantum of local plastic strain. The local plastic strain may vary from one STZ to another but it is taken on average to be of magnitude ($\varepsilon$). The macroscopic plastic strain is the cumulative result of many local events. Once flipped, STZs cannot further deform in the same direction. Instead, they are continuously created and destroyed in order to further accommodate plastic strain within the material.

The amount of configurational disorder in the system is characterized by a single state variable: the effective temperature $\chi$. The effective temperature is formally defined as the change in the system potential energy (or volume) per unit change in the system entropy [*Bouchbinder and Langer*, 2009; *Lieou and Langer*, 2012]. A fundamental result in the STZ theory is that the continuous creation and annihilation of the STZs drive their density $\Lambda$ toward a Boltzmann probability distribution $\Lambda \sim \exp(-1/\chi)$ [*Langer*, 2008; *Langer and Manning*, 2008; *Bouchbinder and Langer*, 2009].

The plastic strain rate $\gamma$ is then given by

$$\dot{\gamma} = (\varepsilon_o/\tau_o) R(s,\chi) \exp(-1/\chi), \tag{1}$$

where $\varepsilon_o$ is the average plastic strain increment per STZ, $\tau_o$ is a characteristic time scale, and $s$ is the shear stress. The rate at which STZs induce an infinitesimal plastic slip is given by the rate-switching function $R(s,\chi)$. The form of $R(s,\chi)$ is constrained by the second law of thermodynamics [*Bouchbinder and Langer*, 2009] and is given by

$$R(s,\chi) = \begin{cases} (1 - s_o/s)\exp(s/s_c\chi), & \text{if } s > s_o; \\ 0, & \text{if } s \le s_o. \end{cases} \tag{2}$$

The parameters $s_o$ and $s_c$ are two stress scales for the STZ system. The stress parameter $s_o$ is the minimum flow stress of the granular system. Thermal fluctuations are not sufficient to drive STZ reversal at the granular scale. Hence, $R(s,\chi)$ is nonzero only if $s > s_o$. Previously, it was shown that $s_c = p$ where $p$ is the pressure [*Lieou and Langer*, 2012].

The effective temperature evolves according to the following equation:

$$\dot{\chi} = \frac{s\dot{\gamma}}{s_o c_o}\left(1 - \frac{\chi}{\hat{\chi}(\dot{\gamma})}\right) + \frac{\partial}{\partial z} D\dot{\gamma}\frac{\partial \chi}{\partial z}, \tag{3}$$

where $z$ is the spatial coordinate across the gouge layer thickness.

Equation (3) states that only a fraction of the externally applied work rate $s\dot{\gamma}$ is dissipated to increasing $\chi$ as it is driven toward its steady state value $\hat{\chi}(\dot{\gamma})$ [*Langer and Manning*, 2008]. This fraction is given by $(1 - \chi/\hat{\chi})$. The effective specific heat $c_o$ determines the amount of energy required to increase the effective temperature. The second term on the right-hand side of equation (3) is effective only if $\chi$ is spatially heterogeneous. There, $D$ is the effective temperature diffusion coefficient, and it scales with the square of particle size. Stability analysis [*Manning et al.*, 2007] shows that the feedback between the strain rate and

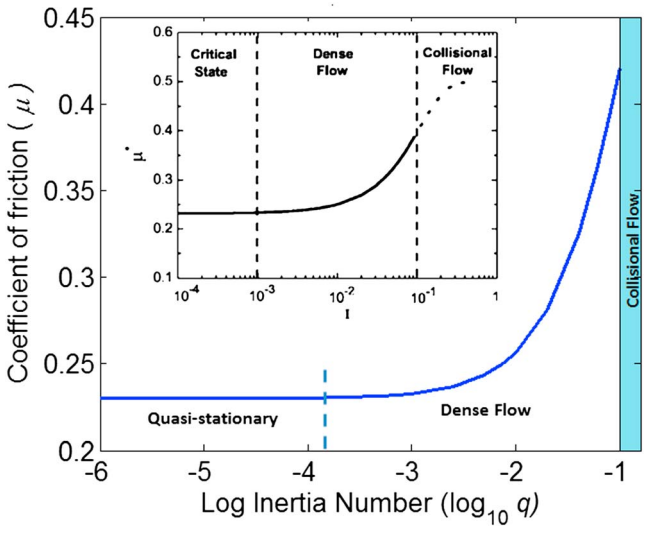


**Figure 1.** Predictions of STZ theory for the rheology of sheared granular system with no local viscoplasticity at grain contacts. Insert shows results from molecular dynamic simulations [*da Cruz et al.*, 2005] (reprinted with permission). (Simulations are shown for $s_o/s_c = 0.23$, $\varepsilon = 1$, and $\chi_o = 0.2$.)

effective temperature may amplify spatial heterogeneities in the effective temperature and ultimately lead to shear banding. Homogeneous deformation corresponds to $\chi(z) =$ constant.

The steady state effective temperature $\hat{\chi}(\dot{\gamma})$ satisfies the following condition: $d\hat{\chi}/dq \geq 0$ where $q = \dot{\gamma}\tau_o$ is the inertia number. The inertia number is the square root of the ratio of the collisional stresses to the pressure. It is widely used to describe the dynamics of dense granular flows [*Da Cruz et al.*, 2005; *Jop et al.*, 2006]. The time scale $\tau_o$ will be chosen consistent with the definition of the inertia number, as we will discuss shortly. Steady state simulations of glassy materials [*Haxton et al.*, 2007; *Langer and Manning*, 2008] suggest that at high strain rates $\chi(\dot{\gamma})$ is given by

$$\hat{\chi}(\dot{\gamma}) = \frac{A}{\ln(q_o/q)}, \tag{4}$$

where $q_o$ is the inertia number at which the effective temperature diverges. In this limit the system fluidizes, and a solid-like description like the STZ theory is no longer applicable. The value of $q_o$ is estimated to be of the order 0.1–1 [*Roux and Chevoir*, 2005]. At low strain rates, the steady state effective temperature can be approximated by a constant value $\chi_o$ that is independent of strain rate. The rate parameter $A$ determines whether the granular system is rate strengthening or rate weakening. Numerous experimental and numerical models for systems of hard and soft spheres under isothermal conditions predict rate strengthening response [*da Cruz et al.*, 2005, and references therein]. We choose a value of $A$ consistent with these observations.

A typical strain rate dependence for the steady state shear stress of a system of hard spheres is shown in Figure 1. No local plasticity at the grain level is considered, and the system is assumed to deform under isothermal conditions. Three major flow regimes are identified in this case. In the quasistatic regime, prevailing at very low strain rates, the shear stress is almost independent of the strain rate. In the dense regime the shear stress increases with increasing strain rate. In the collisional flow regime, prevailing at high strain rates, kinetic energy due to collisional interaction between the particles becomes no longer negligible and STZ theory breaks down. In this limit, a hydrodynamic description is more relevant [*Campbell*, 1990].

The transition from quasistatic to dense flow depends on the properties of the granular system. This is shown in Figure 2 where the value of the parameter $s_o$ is varied. The transition to dense flow occurs at a higher inertia number for systems with higher $s_o$. Figure 2 suggests that varying $s_o$ alone not only alters the strength at low strain rates but it also leads to different strengthening rates at intermediate and high strain rates.

The parameter $s_o$ plays a central role in STZ theory. If a stress lower than $s_o$ is applied to the system, the system undergoes a transient deformation, but it eventually stops. In this limit, the force chains rearrange themselves and always find a stable configuration to resist the applied stress. For stresses higher than $s_o$, the force chains continuously collapse and reform but no stable configuration is achieved. Accordingly, a nonvanishing plastic strain rate is generated [*Bouchbinder and Langer*, 2009; *Lieou and Langer*, 2012]. The value of $s_o$ is a function of many system variables such as grain shape and surface roughness, physical chemistry of the particles, temperature, and existence of fluids.

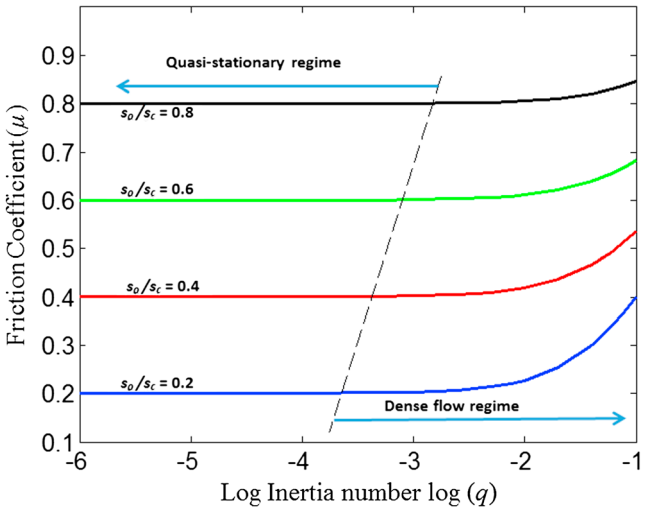


**Figure 2.** Variation of coefficient of friction $\mu$ as a function of inertia number $q$ for different values of $s_o$ normalized by the pressure $s_c$. Systems with higher $s_o$ exhibit a transition from quasistatic to dense flow at higher strain rates. This transition is traced approximately by the dashed curve. The dense flow regime also has different strengthening rates for different values of $s_o$. (The same parameters are used here as in Figure 1 but with different ratios of $s_o/s_c$.)

Different mechanisms contribute to flow resistance in granular systems. These include frictional sliding, particle interlocking, and rolling friction. If the grains are not perfectly spherical, as it is the case with most natural gouge particles, frictional sliding between particles dominates. In that limit, it is possible to relate the value of $s_o$ to the local frictional strength, and hence viscoplastic processes, at the grain contacts. To induce local plastic slip and rearrangements, a force chain must buckle. This is possible if two particles in the chain slide are relative to one another. This in turn requires that the local stress at the particle interfaces exceeds the frictional strength. The local stress and the macroscopic stress are related by

$$sA = s_l A_r, \tag{5}$$

where $A$ is the apparent contact area (of order the particle cross-sectional area), $A_r$ is the real contact area, and $s_l$ is the local stress at the contact level. Similarly, one may assume that the parameter $s_o$ is related to the flow strength at the contact level by an analogous relation

$$s_o A = s_{\text{th}} A_r, \tag{6}$$

where $s_{\text{th}}$ is the flow strength at the contact level. Equation (6) establishes a correspondence between the macroscopic yield stress $s_o$ and the local flow strength

$$s_o = s_{\text{th}} \frac{A_r}{A}. \tag{7}$$

This is an important constraint for grains with viscoplastic contacts. Combining equations (5) and (6), we conclude that $s/s_o = s_l/s_{\text{th}}$. Accordingly, no persistent plastic deformation ($s > s_o$) is possible unless the local frictional strength is exceeded. We discuss this further, in the context of other contact models, in section 5.

The ratio $A_r/A$ depends on pressure $s_c$ and the compressive strength of the grains. At the scale of microcontacts, the compressive strength is of the order of the indentation hardness $H$ of the grains [*Rice*, 2006; *Noda*, 2008]. It then follows from equilibrium of normal stresses that $A_r/A = s_c/H$. The indentation hardness depends on temperature; it decreases as the temperature increases. We ignore the modest evolution of hardness as a function of temperature in this study.

## 3. Viscoplasticity at the Grain Contacts

To complete the temperature-dependent STZ model, we need to define an evolution law for the local flow strength at the grain contacts. Different possible mechanisms for plastic deformation at that scale exist. The dominant mechanism depends on many parameters such as temperature, pressure, and grain size. On the macroscopic scale, the granular system is amorphous with no long-range order associated with grain positions. Locally, however, the grains are crystalline solids susceptible to deformation by dislocation motion. For olivine, as an example, the dominant plasticity mechanism at high stresses and low temperatures is found to be dislocation glide [*King and Marone*, 2012]. As the temperature increases, other mechanism may come into play such as diffusion creep, in which diffusion of vacancies lead to dislocations climbing over pinning sites in the lattice [*King and Marone*, 2012]. Eventually, the local temperature will be high enough to melt some of the minerals in the grains leading to a significant drop in the contact frictional strength [*Rice*, 2006].

To model dislocation glide, we follow *Goetze* [1978] and adopt the following formulation for the flow strength at the grain contacts:

$$s_{\text{th}} = \sigma_p \left[ 1 - \left( \frac{-RT}{\Delta H} \ln \frac{\dot{\gamma}}{B} \right)^{1/q} \right], \tag{8}$$

where the Pierel's stress $\sigma_p$ = 8.5 GPa, the gas constant $R = 8.314$ J/(mol K), the activation enthalpy $H = 5.4 \times 10^5$ J/mol, the empirical constant $B = 5.7 \times 10^{11}$ s$^{-1}$, and the exponent $q$ is taken equal to 2.

At high slip rates, heat is generated at the contact surface faster than it can diffuse. It follows that the local temperature increases and may be high enough to generate a thin layer of molten material at the contact surface or at least melt some of the minerals in the grain. This layer lubricates the interface and reduces the local frictional strength to nearly zero. The occurrence of this flash melting depends on the grain size, the porosity of granular layer, the background temperature, and the melting temperature of the grain constituents. There is also some evidence that the strong degradation in the asperity strength may start at temperatures slightly lower than the overall melting point of the grain contact due to the melting of some of its minerals [*Rice*, 1999; *Tullis and Goldsby*, 2003; *Rice*, 2006; *Beeler et al.*, 2008]. For this purpose, we assume the following empirical formula that connects the low-temperature plastic strength of the asperity with the high-temperature flow strength:

$$s_{\text{th}} = \sigma_p \left[ 1 - \left( \frac{-RT}{\Delta H} \ln \frac{\dot{\gamma}}{B} \right)^{1/q} \right] f(T, T_w), \tag{9}$$

where $T_W$ is the characteristic weakening temperature of the grain mineral and $T$ is the local contact temperature. It is given by $T = T_b + \Delta T$, where $T_b$ is the background temperature and $\Delta T$ is the local rise in temperature.

The function $f(T, T_w)$ is proposed to capture the degradation of the asperity contact strength at elevated temperature. We assume that $f(T, T_w) = 1$ for $T < T_w$. In this limit, equation (9) coincides with equation (8). On the other hand, for $T \gg T_w$, the strength function $f(T, T_w)$ should asymptotically approach zero. The rate of strength degradation depends on many factors such as the chemical environment, the grain metallurgy, and the melting characteristics of the grain constituents. The specific form of $f(T, T_w)$ may be constrained from experiments or numerical simulations as we will discuss in section 6. We emphasize, however, that $T$ in equation (9) is the total temperature at the grain contact which is the sum of the background temperature and the rise in temperature due to the flash heating processes. It follows from equations (7) and (9) that the minimum flow stress $s_o$ is given by the following:

$$s_o = \sigma_p \frac{s_c}{H} \left[ 1 - \left( \frac{-RT}{\Delta H} \ln \frac{\dot{\gamma}}{B} \right)^{1/q} \right] f(T, T_w). \tag{10}$$

Several models were proposed to describe viscoplasticity in crystalline materials. These include the simple Arrhenius-based activation model [*Chester*, 1994; *Nakatani*, 2001; *Rice et al.*, 2001; *Noda*, 2008], the Steinberg-Cochran-Guinan-Lund flow stress model [*Steinberg et al.*, 1980], the mechanical threshold stress flow model [*Follansbee and Kocks*, 1988], and the Preston-Tonks-Wallace flow stress model [*Preston et al.*, 2003]. In these last three models, the flow stress is expressed as a sum of two terms: an athermal component and thermal one. The thermal component of the flow stress is the product of two terms. The first one is the component of the flow stress due to thermally activated processes (e.g., dislocation motion). The second term takes the form $\mu(p, T)/\mu_o$ where $\mu(p, T)$ is the pressure and temperature-dependent shear modulus and $\mu_o$ is a reference shear modulus. Equations (9) and (10) have a similar construction. There, the thermally activated component of the flow stress is given by the dislocation creep model (equation (8)). Accordingly, we hypothesize that the function $f(T, T_w)$ may be reflecting thermal variation in the shear modulus of the region in the vicinity of the grain contacts. Constructing the function $f(T, T_w)$ from first principles is beyond the scope of this paper, but we give an example for a plausible form in section 6.

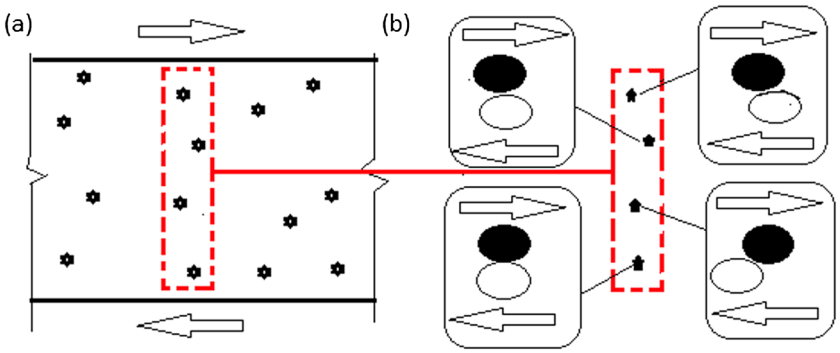


**Figure 3.** A schematic for a 2-D-sheared granular layer with local plastic zones represented by stars. (a) The 2-D representation. STZs are distributed along the depth as well as the width of the sample. The arrow represents the direction of shear. (b) The idealized 1-D model assuming an infinite strip. Local plastic deformation is accommodated by interparticle slip as shown in the oval inserts. At any given instant, different particles are at different stages of their slip history.

## 4. Single Contact Temperature Model

We assume that all contacts are initially at the background temperature $T_b$. The increase in temperature due to local shear heating at the grain contact is computed as follows. The heat generation rate per unit area during sliding is given by $s_l V = sA/A_r V^* = sH/s_c V^*$, where $V^*$ is the local slip rate. This heat source is assumed to be confined to the plane of contact. By convolving the fundamental solution of the heat diffusion equation with this planar heat source [*Rice*, 2006], the temperature rise at the interface is given by

$$\Delta T = \frac{1}{2\rho c\sqrt{\pi\alpha_{\mathrm{th}}}} \int_t^{t+\Delta t} \frac{s(t')V^*(t')}{\sqrt{t-t'}} \frac{H}{s_c} \mathrm{d}t'. \tag{11}$$

The absolute temperature of the contact is then given by

$$T = T_b + \Delta T. \tag{12}$$

When the heat generation rate is constant, the maximum temperature rise occurs at the end of the contact lifetime, i.e., at $\Delta t = a/V^*$ where $a$ is the grain size. This maximum rise is given by

$$\Delta T_{\mathrm{max}} = \frac{sV^*H}{2s_c\rho c\sqrt{\pi\alpha_{\mathrm{th}}}} \sqrt{a/V^*} = \frac{sH}{2s_c\rho c} \frac{\sqrt{aV^*}}{\sqrt{\pi\alpha_{\mathrm{th}}}}. \tag{13}$$

For general time-dependent heat sources, equation (11) is integrated numerically. If the slip rate at the grain contact is not constant, the contact time is defined implicitly through the integral

$$\int_t^{t+\Delta t_c} V^* \mathrm{d}t = a. \tag{14}$$

## 5. Assembly of Contacts

As the gouge layer is sheared, many grains are actively sliding past one another. These grain contacts are at different stages in their slip history; while two grains may be at the end of their contact lifetime, another pair may be just starting the process (Figure 3). In the one-dimensional idealization, adopted here, all STZs are arranged in series with respect to the direction of shear stress. That is, the macroscopic plastic strain rate is the sum of the individual microscopic plastic strain rates of the STZs. The shear stress for all STZs is the same, however. This is analogous to a chain of grains that is sheared at one end. This has two implications. First, the slip rate at the grain contact is not, in general, equal to the imposed slip rate. Compatibility of macroscopic and microscopic deformations dictates that $N\Lambda V^* = \dot{\gamma} h = V$, where $N$ is the number of particles across the gouge layer thickness $h$ or equivalently

$$V^* = \dot{\gamma} a/\Lambda. \tag{15}$$

Here we made the assumptions that all grain contacts slide at the same rate $V_{\mathrm{STZ}}$. Furthermore, we have let $a = h/N$. Second, the minimum flow stress in the system $s_o$ is controlled by the sliding site with the highest

**Table 1.** List of Parameters Used in the Extended STZ Model

| Parameter | Description | Value | Remark |
|---|---|---|---|
| $\varepsilon_o$ | STZ plastic strain | 1.0 | Fitting parameter |
| $a$ | Nominal grain size | 1, 10 μm | Constrained by sample particle size distribution |
| $h$ | Layer thickness | 1 mm | Constrained by experiments/field observations |
| $s_c$ | Confining pressure | 0.5, 75 MPa | Constrained by experiments or depth |
| $c_o$ | Effective heat capacity | 1 | Fitting parameter |
| $\chi_o$ | Steady state effective temperature | 0.15–0.30 | Fitting parameter |
| $\sigma_p$ | Pierel's stress | 8.5 GPa | *Goetze* [1979] |
| $R$ | Gas constant | 8.314 J/mol K | *Goetze* [1979] |
| $\Delta H$ | Enthalpy | $5.4 \times 10^5$ J/mol | *Goetze* [1979] |
| $H$ | Contact hardness | 6 GPa | *Noda* [2008] |
| $B$ | Empirical constant | $5.7 \times 10^{11}$ $s^{-1}$ | *Goetze* [1979] |
| $q$ | Exponent in the dislocation creep law | 2 | *Goetze* [1979] |
| $\rho$ | Grain density | 2700 kg/$m^3$ | *Rice* [2006] |
| $\rho c$ | Volumetric heat capacity | 2.7 MJ/$m^3$K | *Rice* [2006] |
| $\alpha_{\text{th}}$ | Thermal diffusion coefficient | $10^{-6}$ $m^2$/s | *Rice* [2006] |
| $T_w$ | Weakening temperature | 1000, 1300 K | *Rice* [2006] |
| $r$ | Coefficient in the flash heating function (equation (18)) | 2 | Fitting parameter |
| $T_b$ | Background temperature | 300 K | Constrained by experiments or depth |
| $T_r$ | Reference temperature in the flash heating function (equation (18)) | 300 K | Fitting parameter |

temperature or equivalently the lowest strength. This latter conclusion follows from the chain analogy; under uniform stress, a chain breaks at its weakest link. Equations (15) and (13) imply that the rise in temperature for gouge particles depends not only on the grain size but also on the degree of disorder in the system, as given by $\Lambda^{\text{eq}}$. This is an important difference between sliding on a rock surface and sliding by shearing a gouge layer.

## 6. Parameter Selection

Two sets of parameters are used in the current model. The first set relates to the parameters of the STZ theory. The other set is related to the thermal properties of the gouge particles.

For the STZ parameters, we assume that the STZ strain $\varepsilon_o$ is of the order of unity [*Lieou and Langer*, 2012]. This corresponds to the assumption that during local rearrangements, a particle will move a distance that is approximately equal to its size. The inertia time scale $\tau = a/(s_c/\rho)^{0.5}$, where $\rho$ is the grain density, is the time required for a particle to move a distance comparable to its size $a$ under the influence of pressure $s_c$ [*da Cruz et al.*, 2005; *Lieou and Langer*, 2012; *Lieou et al.*, 2014]. This time scale $\tau$ has been found to appropriately describe grain dynamics for a wide range of slip rates. The inertia number $q = \dot{\gamma}\tau$ is the ratio of the plastic strain rate $\dot{\gamma}$ to the strain rate associated with the inertial motion $1/\dot{\tau}$. In applications relevant to seismology, the pressure may be as large as a few hundred megapascal. We take $s_c$ in the subsequent calculations to be equal to 75 MPa unless otherwise stated. The critical inertia number $q_o$, at which the disorder temperature diverges and the inertial flow commences, is assumed to be 0.1–1 [*da Cruz et al.*, 2005; *Roux and Chevoir*, 2005; *Jop et al.*, 2006]. Previously [*Langer and Manning*, 2007], it was shown that in the limit of small strain rates, the steady state value of the disorder temperature approaches a constant value $\chi_o$ that is independent of strain rate. The specific value depends on the nature of the system of particles (e.g., particle shapes and grain size distribution). Numerical simulations of systems of hard spheres suggest that $\chi_o \approx 0.2$ [*Haxton et al.*, 2011; *Lieou and Langer*, 2012]. In subsequent calculations, we vary $\chi_o$ between 0.15 and 0.30. Higher values of $\chi_o$ correspond to less compacted states.

For the properties of the gouge particles, we assume the following nominal values: density $\rho = 2700$ kg/$m^3$, volumetric heat capacity $\rho c = 2.7 \times 10^6$ J/$m^3$k, coefficient of thermal diffusivity $\alpha_{\text{th}} = 10^{-6}$ $m^2$/s, and hardness $H = 6$ GPa [*Rice*, 2006; *Noda*, 2008]. These values weakly depend on temperature. Table 1 summarizes the list of parameters used in this study.

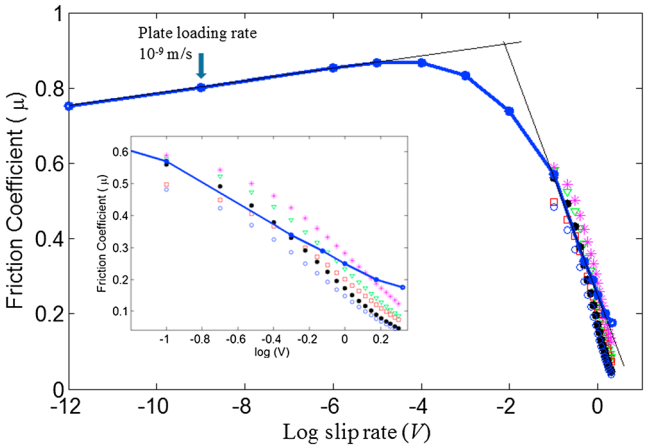


**Figure 4.** Steady state friction coefficient as a function of slip rate (layer thickness = 1 mm) at $T_b = 300$ K. Blue curve represents the prediction of our model based on equation (9) for the grain contact strength. Scattered points represent the sweep of experimental data from *Sone and Shimamoto* [2009]. Different colors correspond to different values for the fitting parameters in *Sone and Shimamoto* [2009].

## 7. Results

To characterize the influence of local heating on the frictional response of the gouge layer, we investigate both the steady state and transient behavior. We also examine the energy partitioning between frictional heat and configurational work.

### 7.1. Steady State Response

If the gouge layer is sheared for a sufficiently long time under constant slip rate, steady state conditions will prevail. That is, no further evolution in the shear stress, plastic strain rate, or disorder occurs. Mathematically, that is equivalent to setting $\dot{\gamma} = V/h, \chi = \hat{\chi}$, and $s = s_{ss}$ in equation (1). The minimum flow stress $s_o$ is calculated based on equation (10) with $T_{ss} = T_b + \Delta T_{ss}$ (equation (12)) where $\Delta T_{ss}$ is the rise in contact temperature at steady state due to local heating. This latter quantity can be estimated from equation (13) by setting $V^* = V_{STZ} = \frac{\dot{\gamma} a}{\Lambda} = \frac{V}{h} a \exp(1/\hat{\chi})$. It follows that

$$\Delta T_{ss} = \frac{s_{ss} H a}{2 s_c \rho c} \sqrt{\frac{\exp(1/\hat{\chi})}{\pi \alpha_{th} h}} \sqrt{V}. \tag{16}$$

Here we have made use of the relation $\Lambda = \exp(-1/\chi)$. The steady state shear stress is then determined by solving the following equation simultaneously with equation (16)

$$\frac{V}{h} = (\varepsilon_o/\tau_o)\left(1 - \frac{s_o(T_{ss})}{s_{ss}}\right) exp\left(\frac{s_{ss}}{s_c \hat{\chi}}\right) \exp(-1/\hat{\chi}). \tag{17}$$

The minimum flow stress $s_o$ is calculated using equation (10), and the form of $f(T, T_w)$ is constrained by experimental measurements.

As an example, we consider the series of high-speed frictional experiments of *Sone and Shimamoto* [2009]. In these experiments, a layer of fault gouge 1 mm thick is sheared at different slip rates in the range of 0.1–2.1 m/s under 0.56 MPa normal stress. They reported that the steady state shear stress varies exponentially with the imposed slip rate. This is represented by the discrete points in Figure 4.

To fit the experimental observations, we solve equations (10), (16), and (17). For this purpose, we make the simplified assumption that the steady state effective temperature is constant and independent of strain rate, i.e., $\hat{\chi} = \chi_o$. This may be justified as follows. The fluidizing strain rate $\dot{\gamma}_c$ corresponding to the experimental conditions discussed here is given by $q_o/\tau$ where $q_o = 1$ and $\tau = a/\sqrt{s_c/\rho} = 6.94 \times 0^{-7}$ s (assuming average grain size $a = 10$ μm). This yields $\dot{\gamma}_c = 1.44 \times 10^6$ s$^{-1}$ which is almost 3 orders of magnitude larger than the highest macroscopic strain rate reported in the experiment (2100 s$^{-1}$). For strain rates that are much lower than the fluidizing strain rates, previous work [*Langer and Manning*, 2007] suggests that the steady state effective temperature is well approximated by its low strain rate limit. We adopt this simplification here and assume $\chi_o = 0.15$. The weakening temperature $T_w$ varies depending on the material composition of the grains. It ranges from 750°C for biotite [*Rice*, 2006] to approximately 1200°C for silicates. Here we choose $T_w = 1300$ K.

For low strain rates, the increase in contact temperature is miniscule (a few degrees) [*Mair and Marone*, 2000; *Mair et al.*, 2006]. In this limit, our theory predicts that the steady state response is rate strengthening (Figure 3). In section 2 we showed that STZ theory predicts rate-independent behavior for sheared granular

**Table 2.** Summary of Equations

| Equation No. | Mathematical Expression | Physical Quantity |
|---|---|---|
| (1) | $\dot{\gamma} = (\varepsilon_o/\tau_o)R(s,\chi)\exp(-1/\chi)$ | Plastic strain rate |
| Embedded in text | $\tau_o = a/\sqrt{s_c/\rho}$ | Inertial time scale |
| (2) | $R(s,\chi) = \begin{cases} (1-s_o/s)\exp(s/s_c\chi), & \text{if } s > s_o; \\ 0, & \text{if } s \le s_o. \end{cases}$ | STZ transition rate |
| (3) | $\dot{\chi} = \frac{s\dot{\gamma}}{s_c c_o}\left(1 - \frac{\chi}{\hat{\chi}(\dot{\gamma})}\right) + \frac{\partial}{\partial z} D\dot{\gamma}\frac{\partial \chi}{\partial z},$ | Effective temperature evolution equation |
| Embedded in text | $\hat{\chi}(\dot{\gamma}) = \chi_o$ | Steady state effective temperature |
| (10) | $s_o = \sigma_p \frac{s_c}{H}\left[1 - \left(\frac{-RT}{\Delta H}\ln\frac{\dot{\gamma}}{B}\right)^{1/q}\right] f(T,T_w)$ | Minimum flow strength |
| (11) | $\Delta T = \frac{1}{2\rho c\sqrt{\pi\alpha_{\text{th}}}}\int_t^{t+\Delta t} \frac{s(t')V^*(t')}{\sqrt{t-t'}}\frac{H}{s_c}\,dt'$ | Local rise in contact temperature |
| (15) | $V^* = \dot{\gamma}a/\Lambda$ | Local slip rate at the grain contact |
| Embedded in text | $\Lambda = \exp(-1/\chi)$ | STZ density |
| (18) | $f(T,T_w) = \begin{cases} 1, & T < T_w; \\ C\exp\left(-r\left(\frac{T-T_r}{T_w-T_r}\right)^2\right), & T > T_w. \end{cases}$ | Flash heating formula |
| (21) | $\dot{s} = G\left(\frac{V}{h} - \dot{\gamma}\right)$ | Stress evolution |

material at low strain rates, and this prediction is consistent with numerical simulation of soft and hard spheres [e.g., *da Cruz et al.*, 2005]. The rate strengthening response shown here has been reported in frictional experiments on fault gouge [e.g., *Chester*, 1994; *Blanpied et al.*, 1995] and has been explained within the framework of rate and state friction [*Dieterich*, 1979; *Ruina*, 1980] which was developed primarily for sliding on rock surfaces. We attribute this behavior to the rate dependence of the contact strength (equation (8)) that overtakes the weakening effect due to temperature changes. Figure 4 suggests that for slip rates smaller than 1 mm/s the steady state friction coefficient depends logarithmically on the slip rate and that $\partial\mu_{ss}/\partial \log V = 0.0075$. Similar values have been documented experimentally [*Dieterich*, 1979; *Ruina*, 1980; *Chester*, 1994; *Blanpied et al.*, 1995; *Marone*, 1997].

To match the behavior at high strain rates, corresponding to $V > 0.1$ m/s, the functional form of $f(T,T_w)$ must be determined. We found the following form to yield the best results (in the sense of absolute error):

$$f(T,T_w) = C\exp\left(-r\left(\frac{T-T_r}{T_w-T_r}\right)^2\right), T > T_w, \tag{18}$$

where $T_r$ is a reference temperature, $T_r = 300$ K, $r = 2$, and $C = \exp(r)$. Expanding the exponential function in equation (18) and defining $T_* = (T-T_r)/(T_w-T_r)$, we obtain the following approximation:

$$f \approx 1 - rT_*^2. \tag{19}$$

In this limit, we recover the temperature-dependent term in the Johnson-Cook flow stress model with $m = 2$ [*Johnson and Cook*, 1983]. This approximation is valid for $T$ in the vicinity of $T_w$. Table 2 gives a summary of the equations for the extended STZ model proposed in this paper.

The predictions of the model fit the experimental measurements very well for slip rates ranging between 0.1 m/s and 1.25 m/s. For higher slip rates, the friction coefficients reported experimentally are lower than what the model predicts. We hypothesize that this discrepancy may be attributed to strain localization which is enhanced at higher slip rates. In the current model, the strain rates are computed assuming a shear zone thickness of 1 mm. *Sone and Shimamoto* [2009] observed that the strain may localize to bands 100–150 μm thick. The strain rate in the shear band is usually higher than the average strain rate [*Manning et al.*, 2007]. The shear band thickness broadens with time [*Manning et al.*, 2007; *Lieou et al.*, 2014], and its

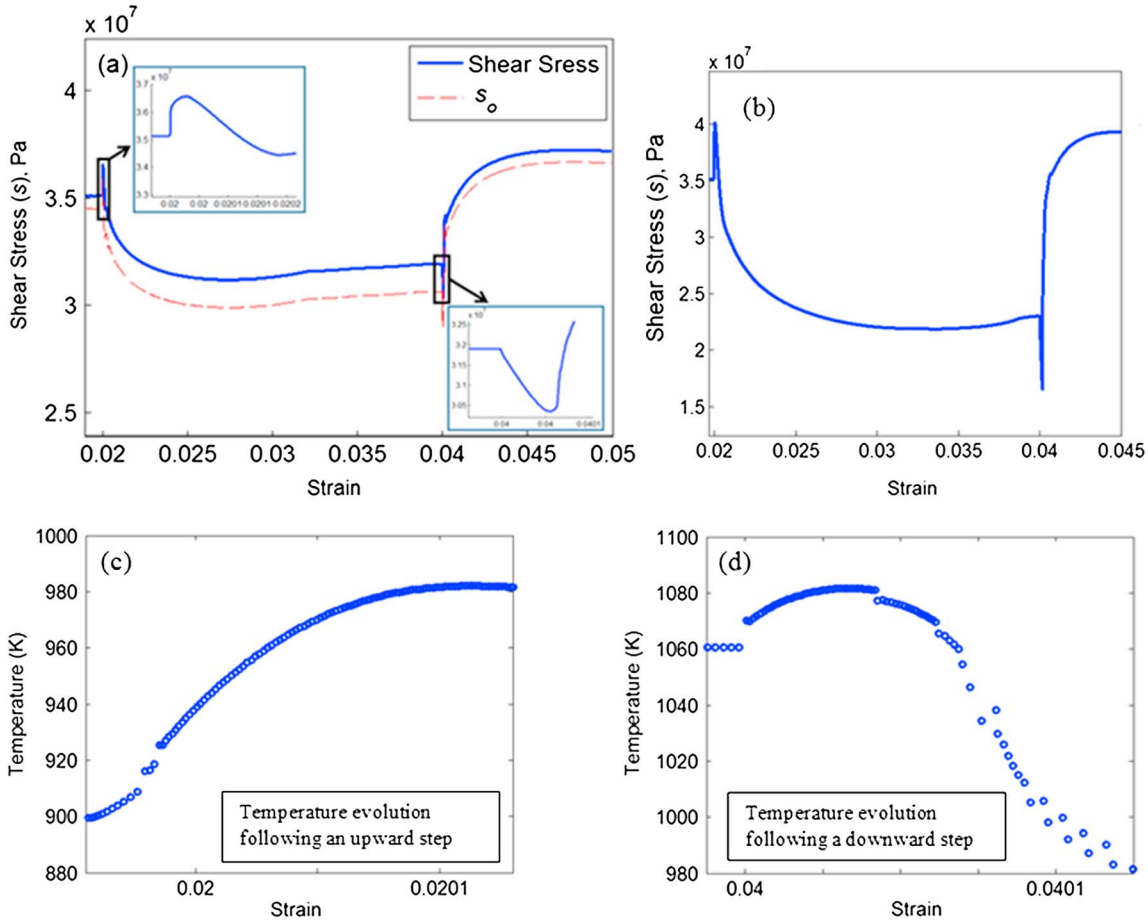


**Figure 5.** Results for a velocity stepping numerical experiment. (a) Evolution of shear stress and minimum flow stress $s_o$. In the upward step, the strain rate is doubled. After steady state is reached, the strain rate was reduced to its original value. Inserts show a magnified plot for the variation of shear stress immediately following the step. Steady state stress is reached after the downward step at strains greater than 0.05 (not shown here). (b) Evolution of shear stress in a pair of strain rate stepping experiment in which the strain rate ratio is 10 (0.1) in the upward (downward) step (respectively). (c) Evolution of contact temperature immediately following an upward step in velocity corresponding to Figure 5a. (d) Evolution of contact temperature immediately following a downward step in velocity corresponding to Figure 5a.

dynamics depend on the imposed strain rate. We expect strain localization to be enhanced at higher slip rates. This in turn leads to larger increases in local temperature and lower flow strength. Thus, we conjecture that modeling strain localization will result in a better quantitative fit for the data at higher slip rates. This will be the subject of a future investigation.

### 7.2. Transient Response

To examine the full response of the sheared gouge layer, including direct and evolution effects, we integrate the STZ equations of motion, equations (1) and (3), coupled with the equation for contact temperature (equation (11)). To complete the dynamical description of the system, we augment the STZ equations by an equation for the evolution of the shear stress

$$\dot{s} = G\left(\frac{V}{h} - \dot{\gamma}\right), \tag{20}$$

where $G$ is the shear stiffness of the system per unit length and $V/h$ is the imposed strain rate. We assume $G = 30$ GPa and consider high strain rates in the range of $10^3$ to $10^4 s^{-1}$. We assume $s_c = 75$ MPa, $a = 1$ μm, $T_b = 273$ K, $T_w = 1000$ K, and $\chi_o = 0.27$. These values lead to reasonable computational cost and are within the range of physically plausible limits for fault gouge. All other parameters are taken as in the previous sections.

#### 7.2.1. Velocity Stepping Experiment

Figure 5a shows the result for a pair of velocity stepping numerical experiments between strain rates $10^3$ and $2 \times 10^3$ $s^{-1}$. The inserts expand the scales to visualize the shear stress variations right after the upward

and downward velocity steps. Several remarks follow from this figure. First, the response is asymmetric for the upward and downward steps. The downward direct effect is slightly larger with a magnitude of 0.154 MPa, whereas the magnitude of the upward direct effect is 0.144 MPa. Second, the evolution of friction following the downward step is steeper than the one following the upward step. Third, following a mathematical step in imposed slip rate, the frictional stress does not follow with an infinite slope as predicted for bare rock surfaces in contact [*Noda*, 2008]. Rather, it gradually evolves, especially in the downward velocity step case.

The previous observations continue to hold for larger changes in strain rates. Figure 5b shows the results for a velocity stepping numerical experiment between $10^3$ and $10^4$ $s^{-1}$. The upward direct effect is equal to 0.5 MPa, while the downward direct effect is equal to 0.64 MPa, compared to 0.144 MPa and 0.154 MPa in the smaller step magnitude experiments, respectively. These results suggest that the normalized direct effect, $\partial s/\partial(s_c \log(V_2/V_1))$, increases with the magnitude ratio of the velocity step $V_2/V_1$.

The asymmetry between the upward and downward direct effect, which increases as the magnitude of the strain rate step increases, may be explained by the thermo-mechanical coupling in our model. As the system is sheared, grains come into and out of contact continuously. Following a velocity step, regardless of its direction, the contact temperature will initially increase. We show in Figures 5c and 5d an example for the temperature evolution corresponding to the stress strain curve in Figure 5a. In case of an upward velocity step, the contact temperature continues to rise (Figure 5c). For a downward velocity step, however, the contact temperature will reach a maximum and then decreases due to the reduced heat generation rate (Figure 5d). This difference in the evolution history of the contact temperature results in different evolution for $s_o$ and consequently different variation in the shear stress. A similar trend was observed in the temperature variations corresponding to the stress strain curve shown in Figure (5b).

A common feature in Figures 5a and 5b is that the evolution of stress as a function of strain, following an upward step in velocity, is nonmonotonic. The stress first decreases until it reaches a minimum and then it increases again toward a steady state. This is explained by the evolution of the local temperature at the grain contacts. Following an upward step in velocity, the contact temperature first increases (see Figure 5c for example). Diffusion effects become important as slip accumulates. Accordingly, the temperature will reach a maximum and then gradually decreases due to heat diffusion. This temperature trend causes the flow stress to first decrease and then increase. The shear stress follows the flow stress trend (Figure 5a).

For a specified velocity stepping protocol, we have found that the stress versus strain relationship describing the gouge layer is independent of the layer thickness. The direct effect is independent of layer thickness, and the slip weakening distance is proportional to the layer thickness (thus, the weakening strain is invariant to the thickness). This observation may not hold true if shear banding occurs. On the other hand, compaction of the layer (as reflected by the initial value of the effective temperature) affects the evolution of the contact temperature, which in turn changes the value of the contact strength, leading to different stress evolution patterns as the system approaches steady state (not shown here). Once steady state is reached at the first driving velocity, the response of the system to subsequent steps in the imposed strain rate appears to be independent of the initial state of disorder. In real faults, variations in imposed strain rates (e.g., from triggered earthquakes) may occur under conditions which are far from steady state, and thus, the corresponding state of disorder would affect the resulting response. Moreover, shear banding patterns depend on the initial state of disorder [*Lieou et al.*, 2014]. A systematic parametric study for the effect of layer thickness and initial sample preparation taking into consideration the possibility of shear banding is a topic of ongoing research.

#### 7.2.2. Velocity Ramps Experiment

The high-speed frictional experiments of *Sone and Shimamoto* [2009] were unique in their ability to test the frictional response under decelerating and accelerating velocity ramps. Figure 6 shows the results of an analogous numerical experiment in which the imposed strain rate increases linearly between $10^3$ and $10^4 s^{-1}$ over a strain of 0.005 and then decreases again to $10^3 s^{-1}$ over a strain of 0.015, after which it remains constant. In this case, it is observed that the upward direct effect is reduced significantly compared to Figure 6. During the upward velocity ramp, the shear stress gradually decreases. The minimum shear stress value is comparable to the minimum value in Figure 5. However, it does not occur at the strain corresponding to the maximum strain rate. The shear stress continues to decrease during a part of the

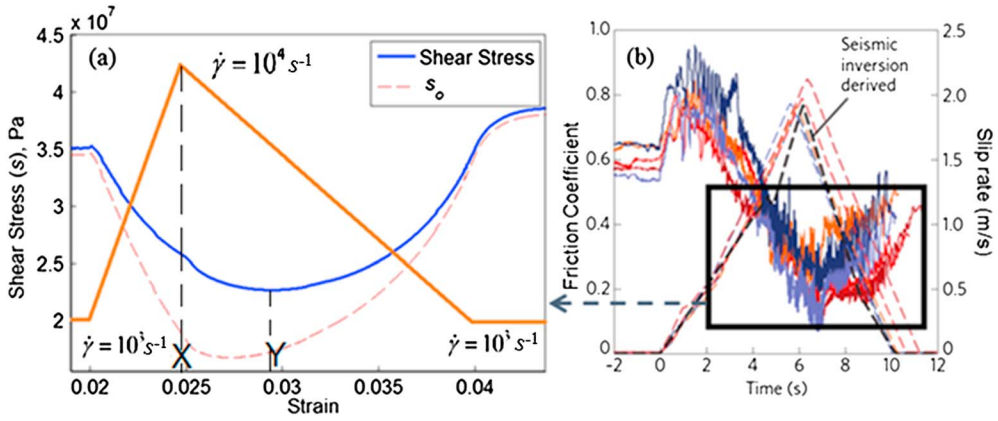


**Figure 6.** Response to linear changes in imposed strain rates. (a) The model predicts gradual weakening followed by gradual strengthening as the velocity is ramped up then down. The brown solid line represents the velocity ramp. (b) Experimental observations from *Sone and Shimamoto* [2009] (reprinted with permission) showing qualitatively similar behavior for the region within the black rectangle.

downward velocity ramp. This is attributed to the reduced value of the minimum flow stress that resulted from the increase in temperature during the upward velocity ramp. Eventually, the shear stress starts to increase while the imposed strain rate is decreasing. The cooling of the asperities due to the reduced heat flux leads to an increase in $s_o$ which in turn results in shear strengthening.

In Figure 6b, we show experimental results from *Sone and Shimamoto* [2009] for a velocity ramping experiment. In their experiment, a shear band of 100–150 μm was observed. Assuming that the strain rate is totally accommodated by deformations within the band, a ramp in the imposed slip rate between 0.1 and 1.0 m/s corresponds to a ramp in strain rates in the shear band from $10^3$ to $10^4$ $s^{-1}$ (assuming shear band thickness 100 um). This is the range of strain rates we tested numerically in Figure 6a. The initial frictional strengthening observed experimentally is due to starting the experiment from zero velocity which requires overcoming the "static friction" in order for the plastic strain rate, and subsequent softening, to start to accumulate. In the numerical model, however, the sample is sheared initially at $10^3$ $s^{-1}$, and by the time the velocity ramp is applied, the system has significantly deformed. Another important difference between the experiment and the numerical model is the pressure scale. The normal stress applied experimentally is of the order of 0.56 MPa which is 150 times smaller than what is used in the numerical simulations. This leads to experimentally longer evolution length and time scales. Nonetheless, the model predictions and the experimental observations show good qualitative agreement in the trend for stress evolution.

### 7.3. Energy Partitioning

In this section we quantify how the energy is partitioned in the gouge layer between its different components. As the gouge layer is sheared, energy is dissipated as radiated energy, frictional heat, and increases in local disorder. The total dissipation is given by

$$E_T = \int s(u)\mathrm{d}u. \tag{21}$$

The configurational energy $E_c$ is the fraction of energy required to change the effective temperature and increase local disorder. The configurational energy per unit area is given by

$$E_c = h\int c_o s_c \mathrm{d}\chi = \int [hc_o s_c \mathrm{d}\chi/\mathrm{d}u]\mathrm{d}u. \tag{22}$$

In this paper we do not consider inertial effects or energy lost to radiation. We thus attribute the remaining dissipation to thermal heating. The heat dissipated per unit area $E_f$ is the difference between the total and configurational energy per unit area,

$$E_f = E_T - E_c = \int [s(u) - hc_o s_c \mathrm{d}\chi/\mathrm{d}u]\mathrm{d}u. \tag{23}$$

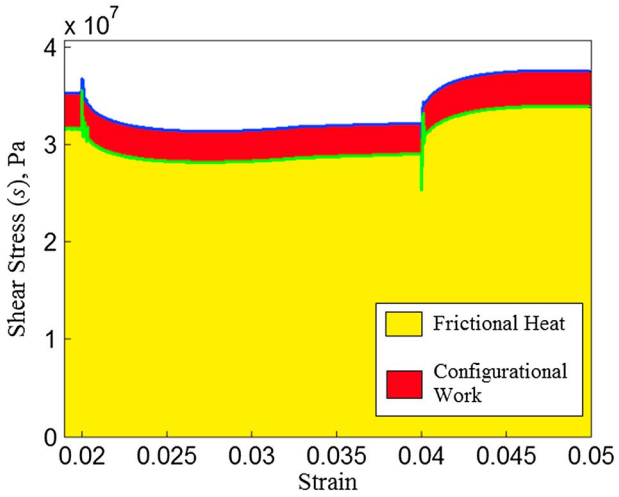


**Figure 7.** Energy partitioning between frictional (yellow) and configurational (red) components. The blue line represents the macroscopic shear stress. The green line represents the fraction of the shear stress that is contributing to heat dissipation. For small strain, as shown here, the configurational energy is approximately 10% of the total energy budget. As slip further accumulates, the effective temperature evolves toward its steady state value and the fraction of energy consumed in increasing local disorder decreases. At steady state, all the external work is dissipated as heat.

An example of the partitioning between these two modes of energy dissipation is shown in Figure 7. The amount of energy dissipated per unit area as frictional heat and configurational energy are represented by the yellow and red areas, respectively. The upper curve in both figures represents the actual shear stress in the system. The boundary between the red and the yellow regions represents the frictional heat stress $s_f$. This is defined as fraction of shear stress contributing to heat generation. From equation (23), this fraction is given by

$$s_f = s(u) - hc_o s_c \mathrm{d}\chi/\mathrm{d}u. \qquad (24)$$

We can immediately see from Figure 7 that configurational energy is not a negligible part of the energy budget. In this particular case, nearly 10% of the dissipated energy is consumed in increasing local disorder. This percentage varies depending on pressure, the initial value of the effective temperature (which reflects how loose or compact the sample initially is), the value of steady state effective temperature, and the magnitude of slip. If the system is sheared long enough to reach configurational steady state, there will be no further increase in the local disorder, and the configurational energy will diminish. In that limit, all work is dissipated as heat.

## 8. Discussion

Several geophysical mechanisms have been proposed to explain the lack of pseudotachylyte materials in exhumed mature fault gouge that would have resulted from rapid recooling of molten rocks if seismogenic heating had been sufficient to cause melting. These include (1) thermal pressurization of pore fluids and (2) flash melting at highly stressed frictional microcontacts [*Rice*, 2006]. In this paper, we implement temperature-dependent viscoplasticity and the theory of flash heating within the framework of shear transformation zone (STZ) theory to predict the frictional response of sheared gouge layers at different slip rates and confining normal stresses.

Important differences exist between sliding on bare rock surfaces and shearing a layer of granular materials. Mainly, granular particles possess extra degrees of freedom compared to asperities on rock surfaces. Grains have both translational and rotational degrees of freedom, and the plastic strain rate is partitioned between these different modes. This further enables grains to rearrange and to accumulate plastic deformation through this process. This flexibility is not available for rock asperities.

For rock surfaces sliding past one another, the asperities on the contact surfaces are arranged in parallel with the shear force. As a result, it is natural to assume that (1) the slip rate at all active asperities is equal to the imposed slip rate and (2) the applied shear force is the sum of the local shear forces at the asperities. It follows that the strength of the interface is the summed resistance of all contacts and is not governed by the weakest one. In this case, the strength is determined by the average contact temperature and not the maximum temperature [*Noda*, 2008].

In sheared granular materials the opposite situation occurs. STZs are arranged in series with the shearing force, analogous to a chain of beads that is loaded at one end (Figure 3). The shear stress may be assumed to be constant across the granular layer so that all STZs are subject to the same stress. The imposed slip rate, however, is partitioned among the active STZs. Accordingly, depending on the STZ density, the local slip

rate at an STZ site may be significantly different from the imposed slip rate. The larger the number of STZs, the smaller the local slip rate compared to the imposed slip rate. Another consequence is that the strength of the system is governed by the strength of the "weakest" STZ. Using the chain analogy and under uniform stress, the strength of the chain is governed by its weakest link. In the context of the current paper, the weakest link corresponds to the sliding site with the smallest local friction or the highest contact temperature.

Other theories for temperature-dependent weakening mechanisms in gouge have been proposed earlier. *Chester* [1994] proposed a state-variable constitutive relation, within Dieterich-Ruina rate and state friction framework, which describes the dependence of friction on temperature near steady state conditions. Their approach is suitable for very low slip rates (μm/s) and is based on the assumption that the micromechanisms of friction are thermally activated and follow an Arrhenius relationship. Here we consider the general umbrella of viscoplastic processes that may occur at the grain contacts at different temperatures and slip rates. By incorporating viscoplasticity within the STZ theory, which takes into account the amorphous nature of the granular layer, we connect the local processes at the grain contacts with the macroscopic plastic strain accumulated by particles slip and rearrangement. The relevant temperature for the activation of the viscoplastic processes is the absolute local temperature at the grain contact. This is the sum of the background macroscopic temperature and the local temperature rise due to flash heating processes. We were able to numerically calculate the changes in temperature at the grain level for different slip rates and to quantify the interaction between thermally activated viscoplasticity and granular dynamics. We showed that this interaction may lead to a nonmonotonic granular rheology. Incorporating these thermally activated processes within the STZ framework will allow us to explore the effect of temperature changes on processes like shear banding which are not directly resolved by the other approaches.

In this paper, we assume that the background temperature is kept constant by continuous cooling. In real faults, this condition is not satisfied in general. Sliding for long distances will inevitably cause an increase in the macroscopic temperature. This will require solving the heat diffusion equation for the background temperature with the heat source term corresponding to the macroscopic heat generation rate $s\dot{\gamma}$. In this case the absolute temperature at the grain contact is calculated by adding the local rise in temperature to the evolving background temperature. The higher the background temperature, the smaller the increase in local temperature required to initiate strong rate weakening. We thus expect that modeling the changes in macroscopic temperature will modify the slip rate at which significant weakening is observed.

The form of the flow rule used here to describe dislocation glide was developed specifically for Olivine [*Goetze*, 1978]. It may be regarded as a special case of the more generalized mechanical stress threshold flow model [*Follansbe and Kocks*, 1983]. At low slip rates, the adopted flow rule predicts changes in frictional strength similar to those observed experimentally (see Figure 3). At high slip rates, the influence of the thermally activated part of the flow rule diminishes as the strength is controlled more by the flash heating processes and the function $f(T, T_w)$. We expect qualitatively similar behavior to be obtained if a simplified Arrhenius relationship [*Chester*, 1994; *Noda*, 2008] is used for the flow rule. The advantage of the mechanical stress threshold model is that it is more flexible and enables the inclusion of microstructure damage evolution at the asperity level. This is relevant for further improvement in the theory.

Granular dynamics is usually described as rate insensitive at low strain rates and rate strengthening at high strain rates. This has been reported in numerous numerical and experimental investigations [e.g., *da Cruz et al.*, 2005]. Fault gouge, however, exhibit viscoplastic properties and was shown experimentally to exhibit both rate strengthening and rate weakening response [*Chester*, 1994; *Blanpied et al.*, 1995; *Sone and Shimamoto*, 2009]. Our modified version of STZ theory with temperature-dependent viscoplastic interactions predicts a modest rate strengthening at low strain rates. At high strain rates, the contact temperature rises significantly. This leads to strong rate weakening that mimics the exponential degradation in strength reported in *Sone and Shimamoto* [2009].

In shearing dry granular layers, dissipated energy is partitioned between frictional heat and configurational energy. The former is responsible for increasing the layer temperature while the latter facilitates local disorder [*Hermundstad et al.*, 2010]. Thermal weakening reduces the total amount of dissipated energy compared to cases when the strength is modeled as a temperature-independent property by reducing the value of the sliding stress at any given strain. Moreover, we have shown that a portion of the total energy,

estimated here to be of the order of 10%, is expended in increasing local disorder. This further reduces the amount of energy dissipated by heat.

Gouge materials at seismogenic depth may undergo interseismic cementation due to physico-chemical reactions expected to operate at elevated pressures and temperatures. The model proposed in this paper assumes a cohesionless granular material. Several factors may reduce the cohesive coupling between gouge particles. These include lack of fluids, reduced pressure at shallow depths, and high-frequency oscillations emitted from the crack tip during earthquake propagation. We hypothesize that the current theory may be extended to include cohesion by (1) modifying the transition rate factors to account for the increased resistance to sliding and flipping due to cohesive bonding and (2) modifying the parameter $s_o$ to include a cohesive strength contribution that is independent of the applied normal stress. This will have an influence on the local velocity at the grain contact, which in turn will impact the temperature increase. We expect, however, that our conclusions would remain qualitatively the same, in that ultimately local shear heating reduces the frictional strength. Developing more precise constraints for the specific form of the rate factors and the minimum flow stress in the presence of cohesion will be the subject of a future investigation.

Depending on the strain rate and grain size distribution, strain may localize to a band that is less than 1 mm thick [*Sone and Shimamoto*, 2009]. Shear banding is as an additional weakening mechanism that affects both the level of the sliding shear stress and the slip weakening distance. STZ theory provides a powerful tool for resolving strain localization at different strain rates [*Daub et al.*, 2008; *Manning et al.*, 2009; *Hermundstad et al.*, 2010]. We expect thermal weakening to enhance the localization process and to affect the dynamics of growth of the shear band.

In continuum systems, a fraction of total energy is dissipated as radiated energy. This additional energy sink was not considered in this paper. We expect systems which weaken rapidly, as a result of thermal weakening, to radiate more energy for the same amount of slip. This in turn will affect the resulting ground motion and in particular its high-frequency content.

Seismic inversions in a number of events, such as the Tohoku earthquake [*Mori*, 2011; *Romano et al.*, 2012], suggest that dynamic rupture propagated for significant distances in what had been identified as rate strengthening regions. Here we considered a rate strengthening granular material as a basic model but showed that thermal weakening, due to local heating of grain contacts, may provide a mechanism by which a material that is rate strengthening at low slip rates significantly weakens at high slip rates. This implies that rate strengthening regions may not always impede rupture propagation. Accordingly, on a fault with both rate strengthening and rate weakening regions, limiting the expected maximum size of an earthquake to the length of the rate weakening zone only could be a dangerous underestimation with serious implications for seismic hazard.

A controlling parameter for the strength of gouge particles with viscoplastic properties is the maximum increase in temperature at the grain contact. The theoretical formulation presented in this paper suggests that this maximum temperature does not depend only on the grain size but also on the state of disorder of the system (see, e.g., equation (16)). Compacted systems are more susceptible to higher increases in temperature. This dependence on the degree of disorder, or the way of sample preparation in terms of looseness or compactness, has no analogy in the case of sliding on bare rock surfaces and is an important characteristic of granular systems

As the material is sheared, two competing mechanisms control the temperature variations: the rate of heat generation and the rate of thermal diffusion. For high slip rates, the former surpasses the latter, and heat is localized, leading to temperature rise and reduction in contact strength. If the slip rate decreases, the effect of thermal diffusion will eventually dominate, leading to a reduction in the temperature. This increases the contact strength and leads to restrengthening. Hence, the temperature dependence of the contact strength allows for both rapid weakening and healing of the sheared gouge layer. This provides a framework for the analysis of constitutive response for different loading rate scenarios, including velocity stepping and ramping experiments, as discussed here, as well as slide-hold-slide tests. In particular, accounting for flash processes at grain contacts may be an important ingredient in understanding the difference in healing rates following low- and high-speed frictional experiments.

Under different combinations of normal stresses and strain rates, grain breakage may become an important weakening mechanism [*Reches and Lockner*, 2010; *Han et al.*, 2011]. *Mair and Abe*, 2008 used three-

dimensional discrete element method to model grain fragmentation processes in fault gouge; they found that grain splitting dominates under high normal stress and at small shear strains, while grain abrasion dominates under low normal stress and at large shear strains. Recently, the shear transformation zone theory was extended to describe shear flow of a disordered granular material that undergoes grain breakage [*Lieou et al.*, 2014]. For the grain size considered in this paper (few micrometers), the threshold pressure above which grain breakage becomes pervasive is of the order of 200 MPa [*Mair et al.*, 2002; *Lieou et al.*, 2014]. This far exceeds the range of normal stresses investigated here (0.5–75 MPa) and renders the effect of grain fragmentation negligible. However, this may not be true at high normal stresses prevailing at seismogenic depths (~10 km). It is thus important in future studies to investigate conditions under which different weakening mechanisms (e.g., flash heating and grain breakage) dominate and how they interplay with one another and affect strain localization in sheared gouge layers.

## 9. Conclusion

In this paper, we developed a model of flash heating in granular materials within the framework of shear transformation zone (STZ) theory to predict the frictional response of sheared gouge layers at different slip rates and confining normal stresses. The theory enables the calculation of the local slip rates at the grain contacts as a function of imposed strain rate and the state of disorder in the system. Using this formulation, the local temperature rise is estimated and its influence on the contact strength is calculated. Our main findings are summarized as follows:

1. The local slip rate at the grain contact is not necessarily equal to the imposed slip rate. The former increases with increasing imposed strain rate and grain size but decreases with increasing disorder (i.e., as the layer dilates).
2. At low strain rates ($< 0.1\ s^{-1}$) the local rise in temperature at the grain contact is minuscule, and the shear strength of the granular layer varies logarithmically with the imposed strain rate. The response may be rate weakening or strengthening depending on the parameters of the viscoplastic flow rule at the grain contact. If the strain rate strengthening in the dislocation creep law overcomes the temperature weakening effect, the response is velocity strengthening and vice versa.
3. At high strain rates ($>100\ s^{-1}$) the local temperature is high enough to cause melting of some of the constituents of the grains. We have found that if the contact strength degrades as an exponential function in the square of the local temperature, the steady state shear strength decreases exponentially with the imposed slip rate. This is consistent with *Sone and Shimamoto* [2009] experimental observations.
4. At intermediate strain rates the local temperature remains below the characteristic weakening temperature for the grain constituents. However, the local temperature is high enough to cause intermediate rate weakening. This is because in this case the temperature softening effect in the dislocation creep flow law overcomes the strain rate strengthening effect.
5. In velocity stepping numerical experiment our model predicts that the downward direct effect is larger than the upward direct effect. The evolution to steady state following a step in strain rate is not monotonic. The nonmonotonicity is related to the evolution of the local contact temperature. Following a step in strain rate, the temperature first increases but then decreases due to diffusion effects. This affects the evolution of contact strength which in turn controls the variation of shear stress as a function of slip.
6. In velocity ramps experiments, our theory predicts a gradual variation in the shear stress as a function of slip. As the imposed strain rate increases, the shear stress decreases and vice versa. The shear stress, however, lacks behind the imposed strain rate. The minimum value of shear stress does not occur at the strain corresponding to the maximum value of imposed strain rate.
7. In a sheared granular material, a fraction of the total energy is dissipated in causing particle rearrangements. This configurational energy sink reduces the fraction of energy to be dissipated as heat and thus help reduce the temperature rise in the layer.

**Acknowledgments**
The authors wish to thank James Langer and Ralph Archuleta for the helpful discussions. The authors also like to thank the Associate Editor and the reviewer for their constructive comments. A.E. Elbanna is grateful for H. Sone and H. Shimamoto for sharing their data and insights into the experimental implications. This research was funded by NSF/USGS Southern California Earthquake Center, funded by NSF 489 Cooperative Agreement EAR0529922 and USGS Cooperative Agreement 07HQAG0008, and by Office of Naval Research MURI grants N000140810747 and 0001408WR20242.

## References

Aagaard, B., and T. Heaton (2008), Constraining fault constitutive behavior with slip heterogeneity, *J. Geophys. Res.*, *113*, B04301, doi:10.1029/2006JB004793.

Ampuero, J. P., and Y. Ben-Zion (2008), Cracks, pulses and macroscopic asymmetry of dynamic rupture on a bimaterial interface with velocity-weakening friction, *Geophys. J. Int.*, *173*(2), 674–692, doi:10.1111/j.1365-246X.2008.03736.x.

Beeler, N. M., T. E. Tullis, and D. L. Goldsby (2008), Constitutive relationships and physical basis of fault strength due to flash heating, *J. Geophys. Res.*, *113*, B01401, doi:10.1029/2007JB004988.
Ben-Zion, Y., and C. G. Sammis (2003), Characterization of fault zones, *Pure Appl. Geophys.*, *160*, 677–715.
Blanpied, M., D. Lockner, and J. Byerlee (1995), Frictional slip of granite at hydrothermal conditions, *J. Geophys. Res.*, *100*(B7), 13,045–13,064, doi:10.1029/95JB00862.
Bouchbinder, E., and J. S. Langer (2009), Nonequilibrium thermodynamics of driven amorphous materials. III. Shear-transformation-zone plasticity, *Phys. Rev. E*, *80*, 031133, doi:10.1103/PhysRevE.80.031133.
Chester, F. M. (1994), Effects of temperature on friction: Constitutive equations and experiments with quartz gouge, *J. Geophys. Res.*, *99*(B4), 7247–7261, doi:10.1029/93JB03110.
Chester, F. M., and J. S. Chester (1998), Ultracataclasite structure and friction processes of the Punchbowl Fault, San Andreas system, California, *Tectonophysics*, *295*, 199–221.
Chester, F. M., J. P. Evans, and R. L. Biegel (1993), Internal structure and weakening mechanisms of the San Andreas fault, *J. Geophys. Res.*, *98*, 771–786, doi:10.1029/92JB01866.
Chester, F. M., J. S. Chester, D. L. Kirschner, S. E. Schulz, and J. P. Evans (2004), Structure of large-displacement, strike-slip fault zones in the brittle continental crust, in *Rheology and Deformation in the Lithosphere at Continental Margins*, edited by G. D. Karner et al., pp. 223–260, Columbia Univ. Press, New York.
da Cruz, F., S. Emam, M. Prochnow, J. N. Roux, and F. Chevoir (2005), Rheophysics of dense granular materials: Discrete simulation of plane shear flows, *Phys. Rev. E*, *72*, 021,309, doi:10.1103/Phys-RevE.72.021309.
Daub, E. G., and J. M. Carlson (2008), A constitutive model for fault gouge deformation in dynamic rupture simulations, *J. Geophys. Res.*, *113*, B12309, doi:10.1029/2007JB005377.
Daub, E. G., and J. M. Carlson (2010), Friction, fracture, and earthquakes, *Annu. Rev. Condens. Matter Phys.*, *1*(1), 397–418.
Daub, E. G., M. L. Manning, and J. M. Carlson (2008), Shear strain localization in elastodynamic rupture simulations, *Geophys. Res. Lett.*, *35*, L12310, doi:10.1029/2008GL033835.
Dieterich, J. H. (1979), Modeling of rock friction: 1. Experimental results and constitutive equations, *J. Geophys. Res.*, *84*(B5), 2161–2168, doi:10.1029/JB084iB05p02161.
Elst, N. J., E. E. Brodsky, P. Y. Le Bas, and P. A. Johnson (2012), Auto-acoustic compaction in steady shear flows: Experimental evidence for suppression of shear dilatancy by internal acoustic vibration, *J. Geophys. Res.*, *117*, B09314, doi:10.1029/2011JB008897.
Falk, M. L., and J. S. Langer (1998), Dynamics of viscoplastic deformation in amorphous solids, *Phys. Rev. E*, *57*(6), 7192–7205.
Falk, M. L., and J. S. Langer (2000), From simulation to theory in the physics of deformation and fracture, *MRS Bull.*, *25*(5), 40–45.
Falk, M. L., and J. S. Langer (2010), Deformation and failure of amorphous solidlike materials. arXiv preprint arXiv:1004.4684.
Follansbee, P. S., and U. F. Kocks (1988), A constitutive description of the deformation of copper based on the use of the mechanical threshold, *Acta Metall.*, *36*(1), 81–93, doi:10.1016/0001-6160(88)90030-2.
Goetze, C. (1978), Mechanisms of creep in olivine, *Philos. Trans. R. Soc. London, Ser. A*, *288*, 99–119.
Han, R., T. Hirose, T. Shimamoto, Y. Lee, and J. I. Ando (2011), Granular nanoparticles lubricate faults during seismic slip, *Geology*, *39*(6), 599–602.
Haxton, T. K., and A. J. Liu (2007), Activated dynamics and effective temperature in a steady state sheared glass, *Phys. Rev. Lett.*, *99*, 195701, doi:10.1103/PhysRevLett.99.195701.
Heaton, T. H. (1990), Evidence for and implications of self-healing pulses of slip in earthquake rupture, *Phys. Earth Planet. Inter.*, *64*, 1–20.
Hermundstad, A., E. G. Daub, and J. M. Carlson (2010), Energetics of strain localization in a model of seismic slip, *J. Geophys. Res.*, *115*, B06320, doi:10.1029/2009JB006960.
Johnson, G. R., and W. H. Cook (1983), A constitutive model and data for metals subjected to large strains, high strain rates and high, in *Proceedings of the 7th International Symposium on Ballistics*, pp. 541–547, The Hague, Netherlands.
Jop, P., Y. Forterre, and O. Pouliquen (2006), A constitutive law for dense granular flows, *Nature*, *441*(8), 727–730.
Kanamori, H., and T. H. Heaton (2000), Microscopic and macroscopic physics of earthquakes, in *Geocomplexity and the Physics of Earthquakes*, American Geophysical Union Geophysical Monograph 120, pp. 147–163, AGU, Washington, D. C.
King, D. S. H., and C. Marone (2012), Frictional properties of olivine at high temperature with applications to the strength and dynamics of the oceanic lithosphere, *J. Geophys. Res.*, *117*, B12203, doi:10.1029/2012JB009511.
Lachenbruch, A. H. (1980), Frictional heating, fluid pressure, and the resistance to fault motion, *J. Geophys. Res.*, *85*(B11), 6097–6112, doi:10.1029/JB085iB11p06097.
Langer, J. S. (2004), Dynamics of shear-transformation zones in amorphous plasticity: Formulation in terms of an effective disorder temperature, *Phys. Rev. E*, *70*, 041502, doi:10.1103/PhysRevE.70.041502.
Langer, J. S. (2008), Shear-transformation-zone theory of plastic deformation near the glass transition, *Phys. Rev. E*, *77*, 021502.
Langer, J. S., and M. L. Manning (2008), Steady-state, effective-temperature dynamics in a glassy material, *Phys. Rev. E*, *76*, 056107.
Lapusta, N., and J. R. Rice (2003), Low-heat and low-stress fault operation in earthquake models of statically strong but dynamically weak faults, Eos Trans. AGU, 84(46), Fall Meet. Suppl., Abstract S51B-02.
Lemaitre, A., and J. M. Carlson (2004), Boundary lubrication with a glassy interface, *Phys. Rev. E*, *69*(6), 061611.
Lieou, C. K. C., and J. S. Langer (2012), Dynamics of sheared hard spheres based on Edward's statistical mechanics and the shear-transformation-zone theory, *Phys. Rev. E*, *85*061308.
Lieou, C. K. C., A. E. Elbanna, and J. M. Carlson (2014), Grain fragmentation in sheared granular flow: Weakening effects, energy dissipation, and strain localization, *Phys. Rev. E*, *89*, 022203.
Lockner, D., H. Naka, H. Tanaka, H. Ito, and R. Ikeda (2000), Permeability and strength of core samples from the Nojima fault of the 1995 Kobe earthquake, in *Proceedings of the International Workshop on the Nojima Fault Core and Borehole Data Analysis, Tsukuba, Japan, Nov 22-23, 1999*, edited by H. Ito et al., pp. 147–152, Open File Report 00-129, U. S. Geological Survey, Menlo Park, Calif.
Lucas, A., A. Mangeney, and J. P. Ampuero (2014), Frictional velocity-weakening in landslides on Earth and on other planetary bodies, *Nature Comms.*, *5*, 3417, doi:10.1038/ncomms4417.
Mair, K., and S. Abe (2008), 3D numerical simulations of fault gouge evolution during shear: Grain size reduction and strain localization, *Earth Planet. Sci. Lett.*, *274*(1), 72–81.
Mair, K., and C. Marone (2000), Shear heating in granular layers, *Pure Appl. Geophys.*, *157*, 1847–1866, doi:10.1007/PL00001064.
Mair, K., F. Renard, and O. Gunderson (2006), Thermal imaging on simulated faults during frictional sliding, *Geophys. Res. Lett.*, *33*, L19301, doi:10.1029/2006GL027143.
Manning, M. L., E. G. Daub, J. S. Langer, and J. M. Carlson (2009), Rate-dependent shear bands in a shear-transformation-zone model of amorphous solids, *Phys. Rev. E*, *79*, 016110, doi:10.1103/PhysRevE.79.016110.

Manning, M. L., J. S. Langer, and J. M. Carlson (2007), Strain localization in a shear transformation zone model for amorphous solids, *Phys. Rev. E*, *76*(5), 056106.

Marone, C. (1998), Laboratory-derived friction laws and their application to seismic faulting, *Ann. Rev. Earth Planet. Sci.*, *26*, 643–696.

Nakatani, M. (2001), Conceptual and physical clarification of rate and state friction: Frictional sliding as a thermally activated rheology, *J. Geophys. Res.*, *106*(B7), 13,347–13,380, doi:10.1029/2000JB900453.

Noda, H., and T. Shimamoto (2005), Thermal pressurization and slip-weakening distance of a fault: An example of the Hanaore fault, southwest Japan, *Bull. Seismol. Soc. Am.*, *95*(4), 1224–1233, doi:10.1785/0120040089.

Noda, H., E. M. Dunham, and J. R. Rice (2009), Earthquake ruptures with thermal weakening and the operation of major faults at low overall stress levels, *J. Geophys. Res.*, *114*, B07302, doi:10.1029/2008JB006143.

Preston, D. L., D. L. Tonks, and D. C. Wallace (2003), Model of plastic deformation for extreme loading conditions, *J. Appl. Phys.*, *93*, 211, doi:10.1063/1.1524706.

Reches, Z. E., and D. A. Lockner (2010), Fault weakening and earthquake instability by powder lubrication, *Nature*, *467*(7314), 452–455.

Rice, J. R. (1980), The mechanics of earthquake rupture, in *Physics of the Earth's Interior*, edited by A. M. Dziewonski and E. Boschi, pp. 555–649, Elsevier, New York.

Rice, J. R. (2006), Heating and weakening of faults during earthquake slip, *J. Geophys. Res.*, *111*, B05311, doi:10.1029/2005JB004006.

Romano, F., A. Piatanesi, S. Lorito, N. D'Agostino, K. Hirata, S. Atzori, Y. Yamazaki, and M. Cocco (2012), Clues from joint inversion of tsunami and geodetic data of the 2011 Tohoku-oki earthquake, Nature, *Sci. Rep.*, *2*, 385, doi:10.1038/srep00385.

Ruina, A. L. (1980), Friction laws and instabilities: A quasistatic analysis of some dry frictional behavior, PhD thesis, Brown University, Providence, R. I.

Scholz, C. H. (2002), *The Mechanics of Earthquake and Faulting*, Cambridge Univ. Press, Cambridge, U. K.

Steinberg, D. J., S. G. Cochran, and M. W. Guinan (1980), A constitutive model for metals applicable at high-strain rate, *J. Appl. Phys.*, *51*(3), 1498, doi:10.1063/1.327799.

Sibson, R. H. (1973), Interaction between temperature and pore-fluid pressure during earthquake faulting: A mechanism for partial or total stress relief, *Nature*, *243*, 66–68.

Sone, H., and T. Shimamoto (2009), Frictional resistance of faults during accelerating and decelerating earthquake slip, *Nat. Geosci.*, *2*, 705–708.

Tullis, T. E., and D. L. Goldsby (2003), Flash melting of crustal rocks at almost seismic slip rates, Eos Trans. AGU, 84(46), Fall Meet. Suppl. Abstract S51B-05.